Applied Clay Science 215 (2021) 106298

Contents lists available at ScienceDirect

Applied Clay Science

journal homepage: www.elsevier.com/locate/clay

Fabrication of novel kaolin-reinforced hydroxyapatite scaffolds with robust compressive strengths for bone regeneration

David O. Obada [a,b,l,*], Sèmiyou A. Osseni [c], Haziz Sina [d], Kazeem A. Salami [a,l], Ayodeji N. Oyedeji [a,l], David Dodoo-Arhin [e], Naresh D. Bansod [f], Stefan Csaki [g], Abdulazeez Y. Atta [h], Opeoluwa O. Fasanya [h,m], Adetunji R. Sowunmi [a,i], Laminu S. Kuburi [a], Muhammad Dauda [a,j], Johnson K. Abifarin [a], Emmanuel T. Dauda [k]

[a] Department of Mechanical Engineering, Ahmadu Bello University, Zaria, Nigeria
[b] Africa Centre of Excellence on New Pedagogies in Engineering Education, Ahmadu Bello University, Zaria, Nigeria
[c] Laboratoire Kaba de Recherche en Chimie et Applications, Faculty of Sciences and Technologies of Natitingou/UNSTIM, Bénin
[d] Laboratory of Biology and Molecular Typing in Microbiology, University of Abomey-Calavi, Benin
[e] Department of Materials Science and Engineering, University of Ghana, Legon, Ghana
[f] Department of Chemistry, Mahatma Gandhi Arts, Science and Late N.P. Commerce College, Armori Dist, Gadchiroli, M.S., India
[g] Institute of Plasma Physics, The Czech Academy of Sciences, Czech Republic
[h] Department of Chemical Engineering, Ahmadu Bello University, Zaria, Nigeria
[i] National Universities Commission, Maitama, Abuja, Nigeria
[j] Air Force Institute of Technology, Nigerian Air Force Base, Kaduna, Nigeria
[k] Department of Metallurgical and Materials Engineering, Ahmadu Bello University, Zaria, Nigeria
[l] Multfunctional Materials Laboratory, Shell Office in Mechanical Engineering, Ahmadu Bello University, Zaria, Nigeria
[m] Industrial and Environmental Pollution Department, National Research Institute for Chemical Technology, Zaria, Nigeria

ARTICLE INFO

Keywords:
Hydroxyapatite
Kaolin
Compressive strength
Trabecular bone
Bacterial strains
Bio-degradability

ABSTRACT

In this study, hydroxyapatite (HAp) microparticles obtained from animal bones were synthesized, and for the first time, HAp was reinforced with beneficiated kaolin using the sol-gel route to improve the mechano-biological properties of the bioceramic materials. The non-reinforced HAp as well as the reinforced samples (K-HAp) were sintered at 900, 1000 and 1100 °C to consolidate the mixture and detailed physico-chemical and mechanical characterizations was conducted. In-vitro experiments in phosphate buffer saline and simulated body fluid were used to confirm the degradability and compatibility of the HAp-derived bioceramic materials, respectively. XRD signatures showed that a dominant phase of hydroxyapatite was formed at all sintering temperatures (900, 1000, 1100 °C). The calcium to phosphate ratio (Ca/P) of the K-HAp-900 sample was approximately 1.67, which is the Ca/P ratio for stoichiometric hydroxyapatite prepared from synthetic sources. The active surface areas of the produced kaolin reinforced bioceramic materials: K-HAp 900–1100,were 0.9770, 0.2159 and 0.8659 m^2/g, respectively, while the obtained micropore volumes were 0.000397, 0.001287, and 0.000334 cm^3/g, respectively. At 900, 1000 and 1100 °C, compressive strengths (after applying the compaction pressure) with a value of 5.67, 6.33 and 7.66 MPa were obtained for the kaolin reinforced bioceramic materials, respectively. The mechanical measurement data further confirms that the reinforced bioceramic materials are suitable for human trabecular bone as the proposed scaffolds were endowed with an improved mechanical strength matching the bearable range of trabecular bone (2–12 MPa). In-vitro experiments showed the degradability and compatibility of the scaffolds. A relative neutral pH was maintained for sample K-HAp 900, and this sample also showed inhibitory potentials for bacterial strain (*E. Coli*).

* Corresponding author at: Department of Mechanical Engineering, Ahmadu Bello University, Zaria, Nigeria
E-mail address: doobada@abu.edu.ng (D.O. Obada).

https://doi.org/10.1016/j.clay.2021.106298
Received 15 May 2021; Received in revised form 25 September 2021; Accepted 27 September 2021
Available online 15 October 2021
0169-1317/© 2021 Elsevier B.V. All rights reserved.

1. Introduction

Critical-sized bone defects represent significant clinical problems that continually drive research in biomedical engineering. Bone implants should be characterized by bioactivity and acceptable mechanical strength. Hydroxyapatite (HAp) is known to be bioactive because it has very close similarities with the mineralogical composition of teeth and bones (Suchanek et al., 1996). However, the mechanical competence of stand-alone HAp is poor which has made the use of HAp limited in clinical settings by reason of this inherent behaviour. Reports revealed that the human trabecular bone has a compressive strength within the range of 2–12 MPa (Jones et al., 2006; White et al., 2007), which has triggered the improvement of the mechanical reliability of HAp through the inclusion of additives such as SiC, Al_2O_3, ZrO_2 and metal fibers (Hongquan et al., 2003). Unfortunately, most additives are detrimental to the biological properties of HAp. Consequently, the inclusion of kaolin and zeolites have gained attention (Harabi et al., 2016; Zhao et al., 2018).

Kaolin, an aluminium silicate, has over time been used as an additive (Mallick et al., 2008; Goyanes et al., 2013), adsorbent (Ballet et al., 2010), and an agent for blood clotting (Véliz et al., 2014). Additionally, kaolin has been identified to facilitate clotting because it enables charge interactions with clotting factors and huge potentials to accelerate haemostasis (Vaiana et al., 2011). An interesting insight in the use of kaolin in the field of pelletization is its plasticizing effect (Law and Deasy, 1997), which was useful in making the hydroxyapatite-based pellets in this study. Kaolin has being reported to be mechanically reliable (Obada et al., 2016c; Obada et al., 2020b), in addition to its non-toxicity. Hence, hypothetically, using kaolin as an additive to reinforce HAp should enhance the mechanical properties without overly comprising the bioactivity.

The application of clay as a naturally occurring material for bone application is gaining attention due to its inherent properties. Noticeable among such studies is the work of Usmaniya et al. (2019), who studied the electrophoretic deposition of bioactive glass nanoclay (kaolin) nanocomposites on titanium. The findings of the study showed an improvement in the corrosion performance of the coating composed of kaolin with the concentration as high as 50% by mass. The results show that kaolinite rich nanocomposites can be regarded as ideal materials for bioimplant coating. Also, Belhouchet et al. (2016) prepared and characterized anorthite from Algerian kaolin and hydroxyapatite from natural phosphate. A composite of kaolin and HAp within the range of 20 to 80 wt% of kaolin was considered, with a sintering temperature within the range of 1000 °C and 1400 °C for the produced samples. The study concluded that the reaction sintering of Kaolin/HAp, anorthite, HAp and mullite materials can be used in different fields. Furthermore, Sutthi et al. (2018), studied the effects of curing temperature and time on the mechanical properties of HAp/calcined kaolin (CK). The curing temperatures were within the temperature of 40 °C and 80 °C and curing time within 2 and 28 days. The result of the study showed that the curing time and temperature significantly affect the compressive strength of HAp/CK samples, and there is no interaction between curing time and curing temperature. By curing the sample at 80 °C for 28 days, the highest compressive strength of 37.8 MPa was achieved. Tang et al. (2014) modified mesoporous bioglass (MBG) with the inclusion of kaolin ranging between 5 and 20% (5-20 k). It was reported that with the addition of kaolin, the MBG-10 K scaffold exhibited a more stable and desirable pH environment, and an enhanced protein adsorption capacity.

In light of these, continued efforts to design novel biological materials is essential in the engineering of bone tissues. These afford insights into the development of man-made and artificial intelligence motivated bioceramic materials with structural and compositional features which have the potential of mimicking natural bone tissues. Reports by Okafor et al. (2020) and Okafor et al. (2021), demonstrated an alternative approach which employs artificial intelligence (AI) based ensemble learning methods for predicting the structural and functional groups of hydroxyapatite (HAp) samples. These may enable the tailored synthesis of robust bioceramic materials with inherent structural and biological properties. Since HAp is quite sensitive to processing protocols, the characterization for specific biomedical applications will suffice for the fabrication of novel bioceramic materials with characteristics suitable as bone implants and essential migration to the clinic.

In light of these, for the first time, the reinforcement of hydroxyapatite with beneficiated kaolin microparticles is reported in this study. In addition, a proposal of a simple protocol which advances a novel approach to fabricate HAp and K-HAp scaffolds by a "low cold compaction pressure" (Abifarin et al., 2019; Obada et al., 2020a; Obada et al., 2021a) technique is presented. Furthermore, the physical, chemical and biological properties, in-vitro, which are important in evaluating the bioactive potentials of the developed bioceramic materials are reported.

2. Materials and methods

2.1. Materials

Animal bones were sourced from an abattoir dumping site in Zaria, Nigeria, and kaolin was collected from a deposit in Kankara, Nigeria. The kaolin was beneficiated by a protocol described by Obada et al. (2016a). The pysico-chemical characteristics of the kaolin (raw and beneficiated) can be found in previous papers of the author's team (Obada et al., 2016a; Obada et al., 2017a; Obada et al., 2017b; Obada et al., 2017c).

2.2. Preparation of hydroxyapatite powder from the animal bones

The animal bones were cleaned to de-proteinize the biomaterials and dried in a hot air oven at 150 °C for 8 h. Afterwards, the bones were subjected to heat treatment in a Nabertherm muffle furnace at 900 °C with a dwell time of 2 h. The bones subjected to heat treatment at 900 °C were grinded and sieved to obtain fine powder with particles lower than 300 μm. The same sample was again sintered (double-stage sintering), after initial sintering, at 900 °C, at temperatures of 900, 1000, and 1100 °C and labelled as HA-900, HA-1000, and HA-1100, respectively. In addition, a non-heat-treated sample was prepared which was labelled as RB (raw bone).

2.3. Microstructure and phase composition

To investigate the phase composition of the raw, synthesized HAp powders and kaolin, XRD patterns were collected on a Bruker AXS, D8 Advance diffractometer operating at 40 kV and 30 mA. The morphology of the beneficiated kaolin and hydroxyapatite powders was observed using a Zeiss Ultra 60 scanning electron microscope which was operated at 15 kV.

2.4. Synthesis and characterization of the kaolin reinforced hydroxyapatite (K-HAp)

The kaolin reinforced hydroxyapatite (K-HAp) was synthesized by the sol-gel method. The already prepared HAp powders (HA-900, HA-1000, and HA-1100) were dissolved separately into 100 ml tap water with stirring for 1 h. Next, the solution of each HAp powder was homogenously mixed with 15 wt% of kaolin particles under continuous stirring for another 1 h. The resultant solutions were mixed with increase in temperature until dryness. The products were further dried at 60 °C for 24 h.

Before pelletizing, to validate the efficacy of the synthesis method (sol-gel) for producing the K-HAp mixture, the morphology of the kaolin mixed hydroxyapatite samples which was only mixed with a spatula before the sol-gel synthesis procedure (BSG), and the resultant K/HAp

powder after the sol-gel synthesis protocol (ASG), was observed using the MAIA3 TESCAN SEM machine equipped with Electron Energy Dispersive X-Ray Analysis (EDX). To investigate the phase composition of the K/HAp samples (ASG and BSG), XRD patterns were collected on a diffractometer (Model: Rigaku, Miniflex 300) operating at 40 kV and 30 mA. A Zeiss EM900 transmission electron microscope was used to establish the grain size of the produced kaolin reinforced HAp (K-HAp). The estimated average crystallite sizes of the kaolin reinforced samples (ASG), in addition to samples produced by spatula mixing of kaolin and hydroxyapatite (BSG), were calculated using the Scherrer broadening method (Scherrer, 1918). The broadening of the reflections can be ascribed to the crystallite size which could be equal or smaller to the grain size (Farzadi et al., 2014). Typically, the (002) HAp reflections were useful for the evaluation (Landi et al., 2000; Farzadi et al., 2011). The Brunauer-Emmett-Teller (BET) method was used to obtain the surface areas and micropore volumes of the reinforced HAp samples using the TriStar 3000 BET analyser. The sintered kaolin reinforced powdery samples were labelled as K-HAp 900, K-HAp-1000 and, K-HAp-1100.

2.5. K-HAp pellets preparation for compressive testing

Next, pelletization of the powders from the sol-gel synthesis was conducted using a pressure of 1 MPa into cylindrical shaped pellets with a diameter of 25.6 mm and thickness of 10.2 mm for hardness and compressive tests. Since the K-HAp pellets required some densification prior to mechanical measurements, the K-HAp samples were sintered at 900, 1000, and 1100 °C at the heating rate of 5 °C/min and a dwell time of 2 h to obtain the representative bioceramic materials.

2.6. Characterization of the physical properties of kaolin reinforced hydroxyapatite

2.6.1. Porosity measurements

Porosity measurements was conducted by adopting Eq. 1:

$$\text{Porosity}\ (\%) = \left(1 - \frac{\text{Weight of Pellet}}{\text{Volume of Pellet} \times \text{Density of Pellet}}\right) \times 100 \quad (1)$$

2.6.2. Density measurements

The theoretical density was calculated based on the expression stated by Kusakabe et al. (2017)

$$\text{Density of the Pellet} = \frac{100}{\frac{\propto}{d_1} + \frac{(100-\propto)}{d_2}} \quad (2)$$

where α = wt% of Kaolin, d_1 is the density of kaolin (2.65 g/cm^3) and d_2 is the Density of HAp (3.16 g/cm^3) (Landi et al., 2000; Ayed et al., 2001; Munar et al., 2006; Obada et al., 2020a).

Dimension of the Pellets:

Average diameter of the pellets = 25.6 mm

Average height of the pellets = 10.2 mm

Measurements were taken in triplicate and the average values were recorded.

2.7. Compressive strengths of HAp and K-HAp pellets

The compressive strengths of the K-HAp scaffolds was measured in triplicates using a TQSM1000 universal testing machine equipped with a 5 kN load cell. A comparison of the compressive strength of the pellets with compaction and no compaction pressures was made.

2.8. Statistical analysis

Statistical analysis was performed using SPSS (Statistical Package for Social Science, SPSS, version 20.0, SPSS, Chicago, IL, USA). After calculating the mean ± standard deviation of the compressive strengths, one-way ANOVA test was used to compare the groups and determine the significance of the effect of sintering temperature on the compressive strength of the compacted and non-compacted samples. In the current study, $p < 0.05$ was considered statistically significant.

2.9. Antimicrobial assessment of the scaffolds

The antimicrobial activity of the kaolin reinforced samples (K-HAp) was conducted using the disc diffusion method (Bauer, 1966) against *Staphylococcus aureus* (*S. aureus)* and *Staphylococcus épidermidis* (*S. epidermis)* as Gram-positive bacteria models, and *Escherichia coli (E. coli)* and *Pseudomonas aeruginosa* (*P. aeruginosa)* as Gram-negative bacteria models. The *Candida albicans* (*C. albicans)* microbial strain was used as the model fungi. The inoculums of the micro-organisms were synthesized via fresh overnight broth cultures which were kept in the incubator at 37 °C under constant stirring. The agar disc diffusion studies were performed using Muller Hinton agar (MH, pH 7.3 ± 0.1), and conducted by pouring the agar into petri plates containing 15 ml of molten media. The turbidity of the bacterial suspension was adjusted to 0.5 Mcfarland standard and with a sterile swab, the bacterial culture was streaked on previously prepared MH agar dish. The paper discs were conditioned separately with 25 ml of the powder prepared previously and placed at equal distance in a circle on the seeded dish. These dishes were placed at room temperature for about 15–30 min before incubation at 37 °C for up to 48 h. After the period of incubation, the dishes were assessed for the inhibitory zones which included the diameter of the discs. Each sample was used in duplicate for the assessment of the antibacterial and antifungal activity. The blank discs were used as a negative control.

2.10. In-vitro biological evaluations (biocompatibility) of the kaolin-reinforced scaffolds

The bioactivity of the prepared pellets was evaluated using a simulated body fluid (SBF) solution which was prepared according to the protocol of Kokubo and Takadama (2006). The pellets representing the synthesized bioceramic materials were placed in an air-tight polyethylene container with a volume of 50 ml SBF solution and carefully positioned in an incubator using a water bath for a period of 7, 14 and 28 days, respectively at 37 °C. The SBF solution was replaced every day during the experiments to preserve ions concentration.

2.11. Biodegradability assessment of the scaffolds

Biodegradability studies were conducted to assess the gradual weight loss of the scaffolds in a phosphate buffer solution (PBS) for 7, 14 and 21 days by dissolving a PBS tablet in 100 ml of deionized water to obtain a pH of 7.4. Each pellet was placed in 50 ml of PBS solution and kept in an incubator. Readings were taken for the pH variation and weight loss of each respective bioceramic pellets before and after the incubation using a pH meter and an analytical balance (accuracy: 0.001 g). The percentage of weight decrease (W_d) was calculated using Eq. 3:

$$\text{Wd} = \frac{W_a - W_b}{W_a} \times 100\% \quad (3)$$

where W_a and W_b are the respective weights of samples before and after soaking in phosphate buffer saline solution, respectively.

3. Results

3.1. XRD patterns of kaolin, raw animal bones and its derived hydroxyapatite

The XRD pattern of kaolin (Fig. 1) exhibits two prominent reflections at 12° and 24.90° 2θ, and other reflections at 19.94°, 35.98° and 55.12°

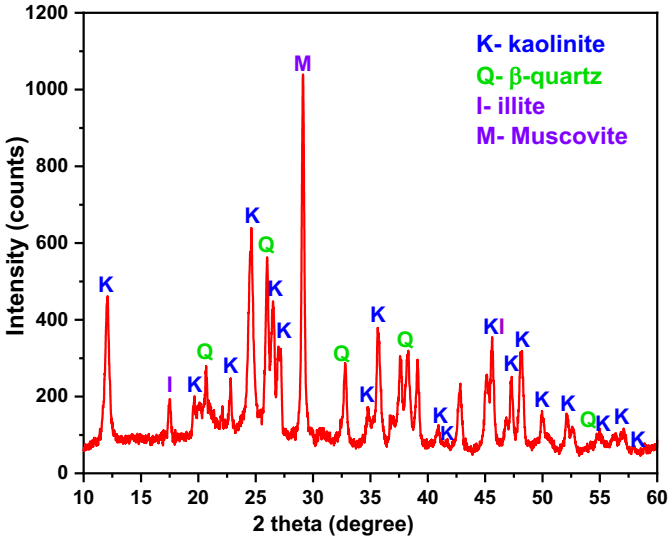

Fig. 1. X-ray diffraction pattern of Kankara kaolin.

2θ. These reflections were matched with the PDF card number 01–089-6538 and buttressed by reports elsewhere (Kakali et al., 2001; Obada et al., 2016b; Obada et al., 2016c). The results indicated that kaolinite was the predominant phase in the powdery bulk. In addition, illite, muscovite and quartz were identified as minor mineral phases present in the sample.

The XRD patterns of the non-reinforced HAp (Fig. 2) represents characteristic signatures of HAp reflections at 26.17, 28.25, 29.1, 31.9, 32.35, 33, 34.2, 39.96, 46.85, 48.25, 50.65, 51.4, 52.35, 53.38 and 63.1° 2θ. All the reflections are common of the hexagonal phase of hydroxyapatite (Chavan et al., 2010; Akpan et al., 2020a; Akpan et al., 2021a) and is in line with JCPDS No. 74–0566 (Heidari et al., 2016). The pattern of raw bones (RB) which is characterized by broad reflections can be attributed to the low crystallinity of the HAp phase.

3.2. SEM images of kaolin, raw bones and raw bones derived hydroxyapatite

Fig. 3(a–d) shows the morphology of kaolin particles at different magnifications. For all the images, the structured layers of kaolinite mineral in kaolin are stacked with an obvious booklet morphology, with particular emphasis on the image taken under the highest magnification (image 3d; 100 kX). These structured layers were also seen to align parallelly showing some discontinuities. These observations are in line with the typical morphology of kaolinite as described by several authors (Bohor and Hughes, 1971; Lee et al., 2003; Bergaya and Lagaly, 2013).

The SEM images and EDX spectra of the raw animal bones and heat-treated variants are depicted in Figs. 4 and 5. Hollow surfaces are observed for the raw bones (RB) while for all the heat-treated (sintered) variants at different temperatures, the particles are closely packed. This can be ascribed to the effect of heat during the sintering regimes (densification). The samples subjected to heat-treatment (HA-900, 1000, 1100) exhibit inter connectivity related to their dense structures and defines the start of a crystalline grain structure of hydroxyapatite (Haberko et al., 2006; Murugan et al., 2006; Zhao et al., 2013; Lowe et al., 2016). The presence/distribution of pores are evident on the surface of the samples with consequent potential application for cell proliferation in orthopaedic medicine (Sopyan and Kaur, 2009). It is worth noting, from the SEM images, that the spherical shaped particles with clumped and agglomerated distribution peculiar to hydroxyapatite is characteristic of the sintered variants.

The EDX spectra in Fig. 5 confirms that HAp is primarily composed of calcium (Ca), phosphorus (P) and oxygen (O) with traces of minor elements. This composition has huge similarities to the chemical constituents of the natural bone (Ramesh et al., 2018)

3.3. Viability of the sol-gel synthesis route: XRD patterns and SEM of BSG (before sol-gel) and ASG (after sol-gel) samples

To gain insight into the efficacy of the synthesis method, XRD and SEM analyses were carried out on the prepared powdery composite (BSG & ASG) as shown in Fig. 6a and b, respectively. Typical reflections with higher intensities at 31.9, 32.35, 33, and 34.2° 2θ, which corresponds to reflections of the hexagonal phase of hydroxyapatite [$Ca_{10}(PO_4)_6(OH)_2$] were observed. The reflections of kaolinite in the two samples were not visible due to the low kaolin content (15 wt%) in the mixture. In addition, due to the non-mesostructured nature of kaolin, the diffraction reflections of the BSG mix broadened slightly and the diffraction intensities decreased to an extent. Correspondingly, the diffraction reflections of ASG were significantly increased at 31.9, 32.35, 33° 2θ. In addition, ASG powders had a higher crystallite size of 98.7 nm compared with BSG powders of 51.6 nm. This infers that ASG powders have the potential to exhibit better mechanical properties, because, with increased crystallite size, ASG powder would be resistant to micro-cracking due to the anisotropic thermal expansion coefficient. After matching the results obtained from the BSG and ASG powders with the JCPDS database, prominent phase of hydroxylapatite and hydroxy-flouroxyapatite were formed respectively, with the formation of hydroxyflouroxyapatite ascribed to the partial substitution of the hydroxyl (OH^-) by the fluoride (F^-) ions which also has the potential to enhance the mechanical properties of the HAp pellets.

Fig. 6b reveals the morphological structure of the spatula mixing (BSG) and the sol-gel-derived kaolin reinforced HAp (ASG). From the representative SEM images of BSG, it is observed that the typical booklet morphology of kaolin was visible between the bead-like morphology of HAp aggregates. This depicts an inhomogeneous mix at both magnifications (10.0kX and 20.0kX). A quite uniform morphology was observed for ASG samples at low and high magnifications with the microstructures mostly composed of the bead-like morphology of HAp. This confirmed the hypothesis that the sol-gel method could improve the homogeneity and enhance the physico-mechanical properties of the kaolin reinforced composite.

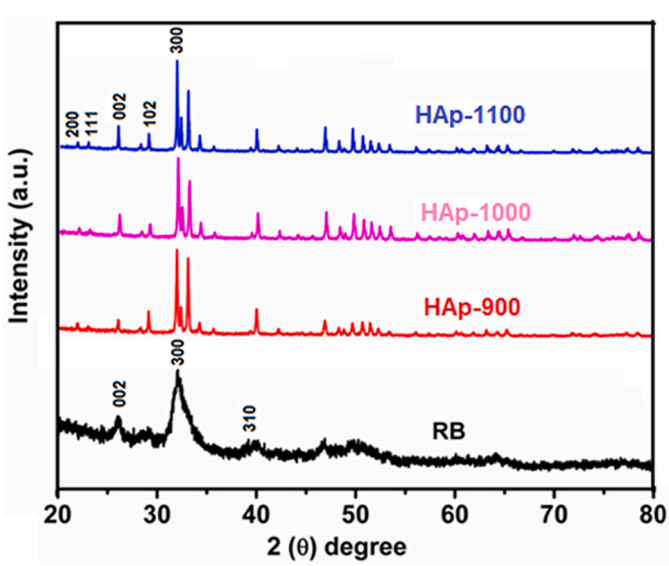

Fig. 2. X-ray diffraction patterns of the synthesized hydroxyapatite (HAp) samples at various sintering temperatures.

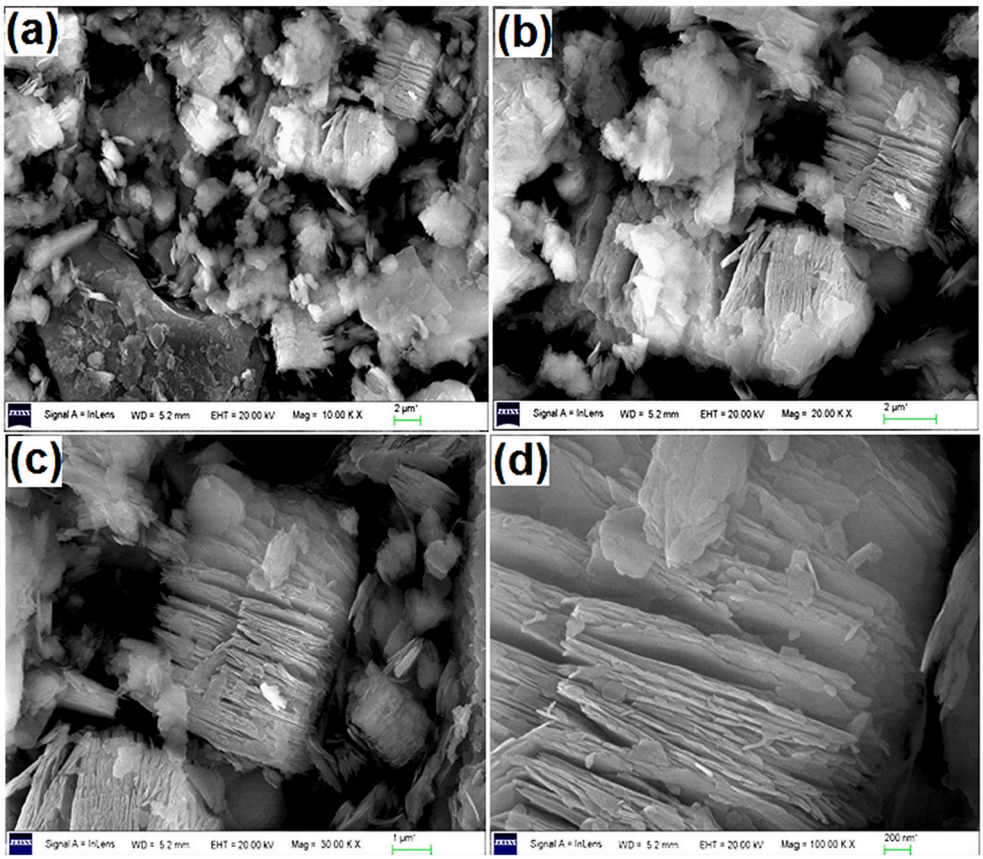

Fig. 3. SEM images of Kankara kaolin at different magnifications, a) 10,000× b) 20,000× c) 30,000× d) 100,000×.

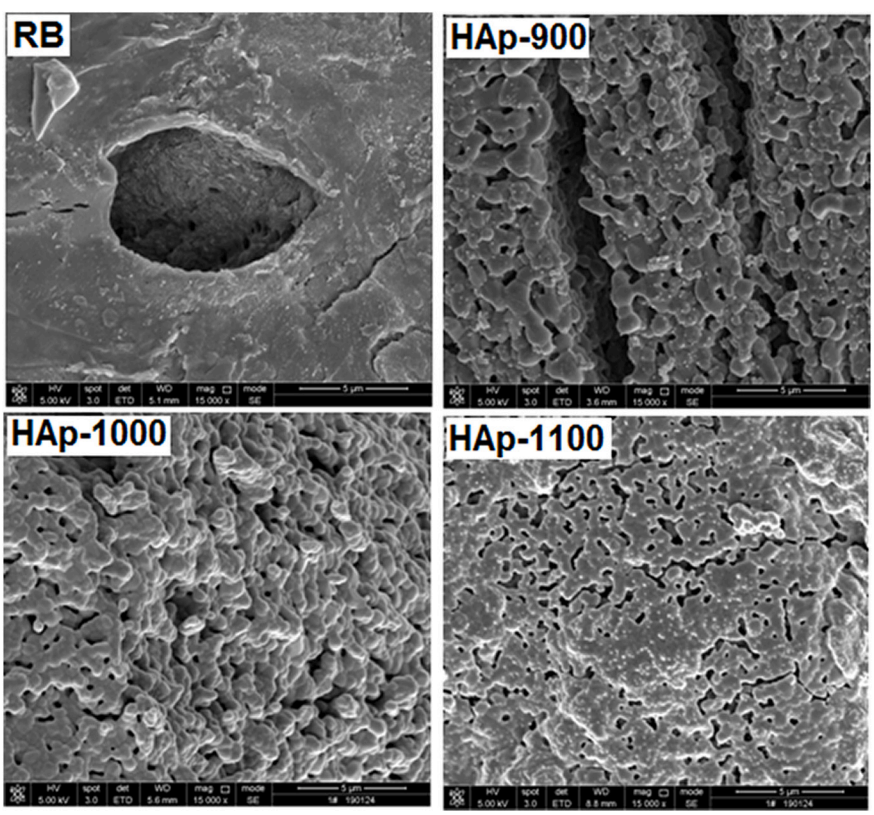

Fig. 4. SEM images of the raw animal bones and hydroxyapatite (HAp) samples sintered at 900, 1000 and 1100 °C.

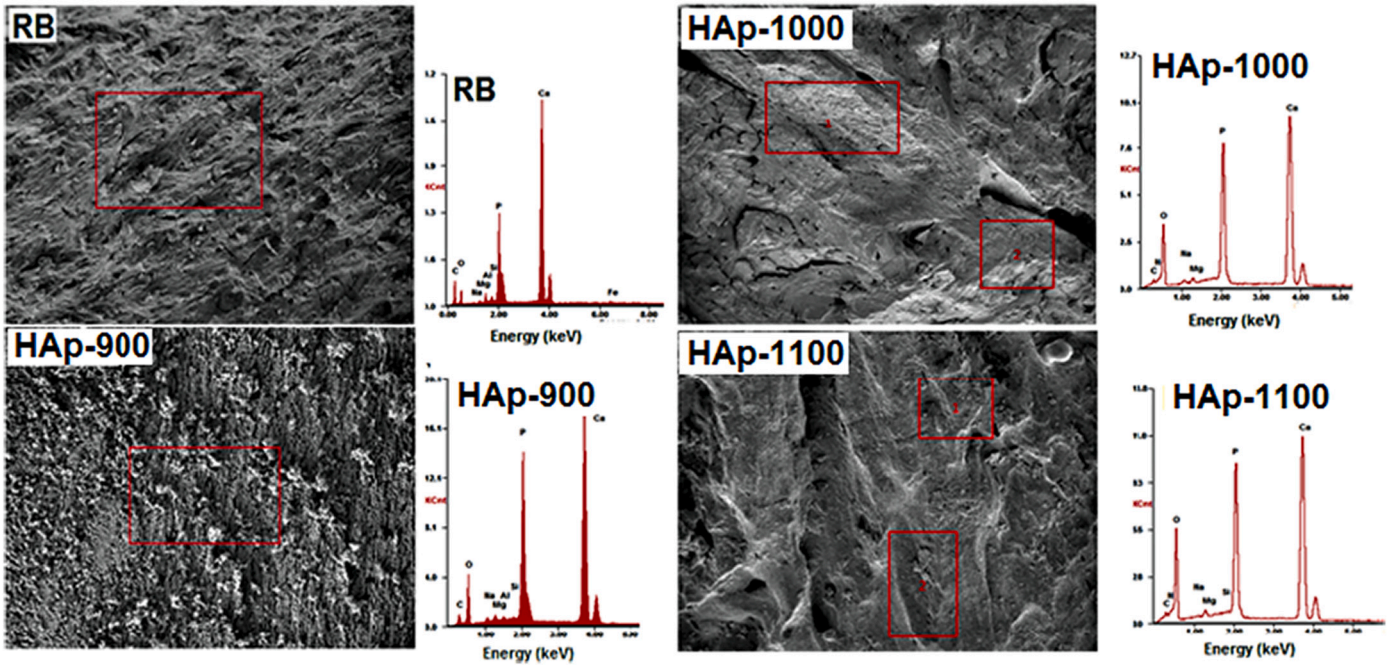

Fig. 5. EDX spectra of the raw animal bones and hydroxyapatite (HAp) samples sintered at 900, 1000 and 1100 °C.

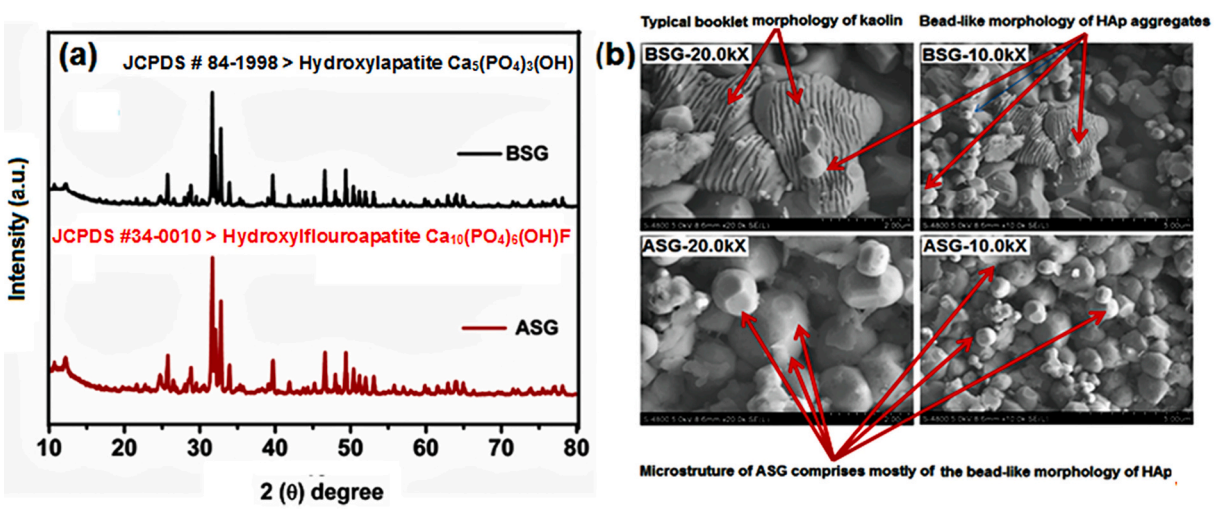

Fig. 6. a) X-ray diffraction signatures of hydroxyapatite (HAp)-kaolin mix before sol-gel (BSG) and after sol-gel (ASG), b) SEM images of BSG and ASG.

3.4. Average crystallite sizes of kaolin and kaolin reinforced hydroxyapatite

The crystallite sizes of kaolin and kaolin reinforced hydroxyapatite were generated by virtue of the (002) reflections from the XRD analyses. The crystallite sizes of the kaolin, K-HAp-900-1100 were 42.61 nm, 45.04 nm, 63.03 nm, and 54.50 nm, respectively. These crystallite sizes are close and comparable to the size of the HAp nanocrystals in natural bone (about 50 nm) as reported by Kikuchi et al. (2001). Rusu et al. (2005) also observed a crystallite size range of 15 to 50 nm for HAp crystals decorated on a chitosan matrix. Relatedly, Pang and Bao (2003), reported a size range of 20 to 53 nm for their as-prepared HAp nanoparticles. As shown in Table 1, it was noticed that the increase in the crystallite sizes with an increase in sintering temperature was not linear. One possible explanation for this could be that the HAp with the largest crystallites in sample K-HAp 1000 was formed mainly due to the formation of larger microcrystals during sintering. As much as macropores in a HAp implant are essential for bone ingrowth, this is also enhanced as bioceramic scaffolding materials also contain microporosity. The results of surface area and micropore volume (Table 1) are quite close to the surface area and pore volume of hydroxyapatite samples as reported by Pramanik et al. (2005, 2007). There is a consistent trend between the surface areas and average crystallite sizes. With increasing sintering

Table 1
Average crystallite sizes of the kaolin reinforced hydroxyapatite (K-HAp) samples.

Sample code	Average crystallite size (nm)	Surface area (m^2/g)	Micropore volume (cm^3/g)
K-HAp-900	45.04	0.9770	0.000397
K-HAp-1000	63.03	0.2159	0.001287
K-HAp-1100	54.5	0.8659	0.000334

temperature of the samples, there is a decrease in surface area for K-HAp-1000 sample. An increase in surface area is noticed as the crystallite size dropped for the K-HAp-1100 sample. The increase in surface area following this trend can be ascribed to smaller crystallites and higher reactivity of particles in the solid. The low surface area of the materials, as reported, can be ascribed to the external surface of the particles of the bulk.

3.5. Representative morphologies and Ca/P ratio of the K-HAp samples

The SEM images of the K-HAp bioceramic materials (Fig. 7a) reveal aluminosilicate crystals which are deposited on the surface of all the samples as spheroidal oriented particulates are merged with more obvious agglomerates which can be ascribed to the addition of kaolin. The nano and micro-sized crystals complimentarily reveal the typical microstructure of HAp. The EDX analysis of K-HAp samples (Fig. 7b) revealed that the Ca/P ratio was within the range of 1.66–1.99, which is close to the Ca/P ratio in natural apatite of hard tissue with similar ratios reported elsewhere (Abifarin et al., 2019; Akpan et al., 2020b; Obada et al., 2020a; Akpan et al., 2021b). The EDX analyses for K-HAp (900–1100) showed the presence of silicon (Si) and aluminium (Al) due to the addition of kaolin. The Ca/P ratio (1.66) of K-HAp-900 was the closest to stoichiometric Ca/P ratio of hydroxyapatite (1.67) among the samples. The Ca/P ratio of K-HAp-900 seem to be a little calcium deficient which may make it highly soluble and as a consequence be better comparatively with the other kaolin-reinforced variants in terms of its osteoinductive support for bone regeneration (Li et al., 2012).

The solid particles noticeable on the TEM images of K-HAp samples (Fig. 7c) are mostly ascribed to HAp. The TEM images revealed that the samples' particles are mostly spherical in shape and in line with other studies (Sun et al., 2006; Lin et al., 2007). This has positive consequences as it has the potential to enhance the mechanical properties of bioceramic materials. It was difficult to further complement the findings from the TEM images with the topographical morphology from SEM as clearer morphological gradients were revealed by SEM.

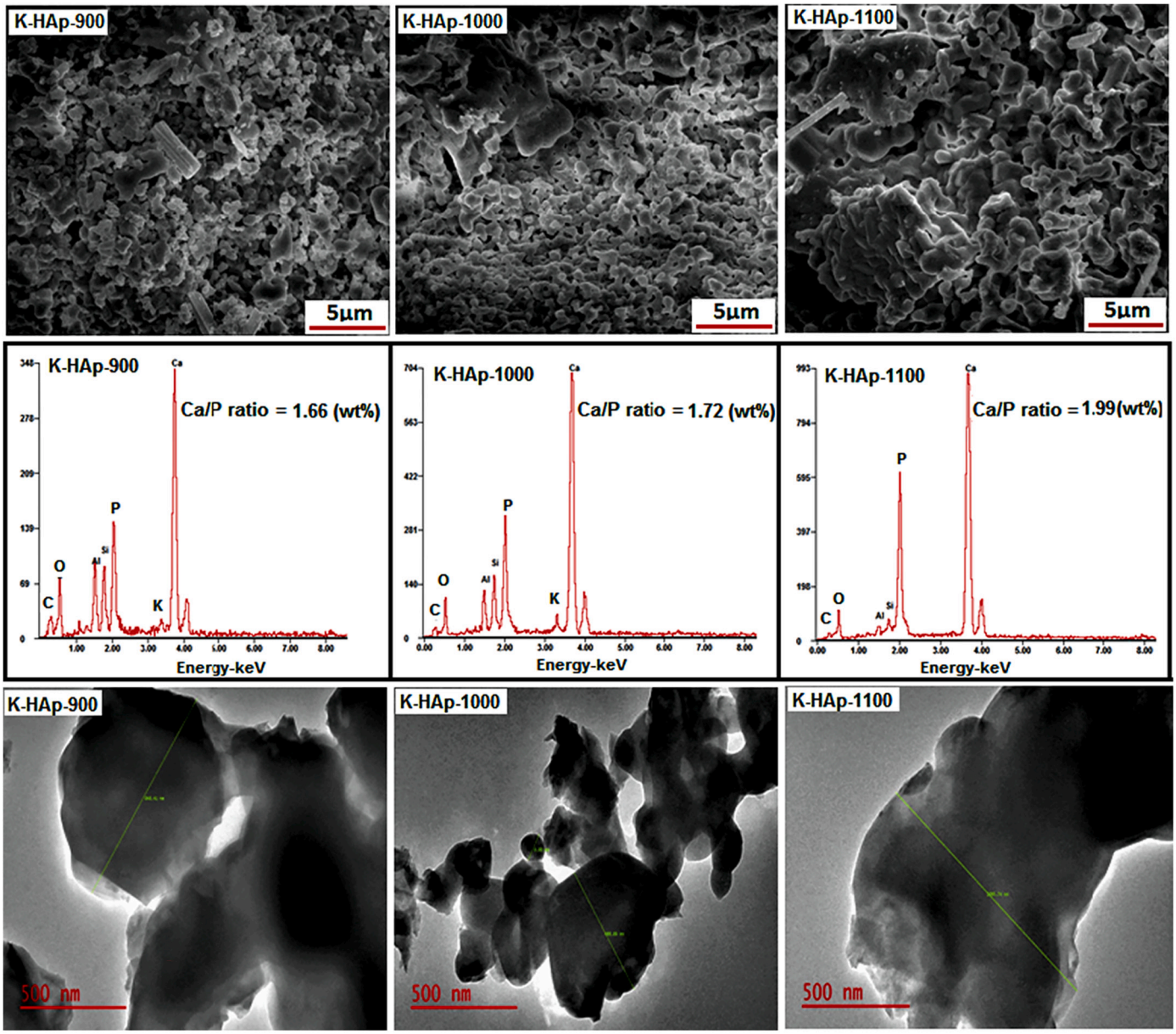

Fig. 7. a) SEM images of the kaolin reinforced hydroxyapatite samples (K-HAp), b) EDX spectra of the K-HAp samples, c) TEM images of the K-HAp samples.

3.6. XRD signatures of K-HAp samples

The XRD patterns of the K–HAp samples after sintering at different temperatures (900–1100 °C) are seen in Fig. 8. The diffraction peaks of the K–HAp mixture sintered at 900 °C are found to be in accordance with the structure of the crystalline hydroxyapatite. However, when the sintering temperature increased to 1000 and 1100 °C, two small reflections could be seen at 31.17° and 34.51° 2θ, and can be identified as β-TCP which has the potential to accelerate new bone formation (Dean et al., 1995), if the bioceramic materials are used as implants. The appearance of β-TCP resulting in the decomposition of HAp at 1100 °C can be ascribed to kaolin containing SiO_2 which reacts with HAp and transforms into the TCP phase. This is in line with the findings reported by Laonapakul et al. (2021). This indicated the lower thermal stability of the K-HAp with an increase in the sintering temperature. As the sintering temperature increased above 1000 °C, the appearance of the transformed phases of kaolin (cristobalite and mullite) were observed. Hydroxyapatite was still a predominant phase at these temperatures, as the reflections were matched with hydroxyapatite card number of 96–900-3549. However, mullite, cristobalite and tricalium phosphate reflections were also noticed with ICDD files: 96-900-1568, 96–900-1579 and JCPDS card number 09–0169, respectively. This implies that at higher sintering temperature, kaolin transformation which is associated with the dehydration and dehydroxylation processes took place. This allowed a reduction of the intensity of the reflections of HAp, especially for K-HAp-1100 sample. These characteristics have implications on controlling microstructure and avoiding exaggerating grain growth which may affect the mechanical strength of the kaolin reinforced scaffolds.

3.7. Physical characteristics of the kaolin reinforced samples

The porosities of K-HAp- 900, 1000 and 1100 are 45.7 ± 0.01%, 45.9 ± 0.01%, and 57.1 ± 0.01%, respectively (Fig. 9). At higher sintering temperatures, the porosity for K-HAp-1000 slightly increased and can be considered very marginal. The porosity for K-HAp-1100 increased, though this trend is not typical for porosities of ceramic materials when subjected to elevated temperatures. One reason for the trend noticed in this study could be that the smaller pores in the bulk of the bioceramic materials were absorbed into larger pores. It has been reported previously that porosity in the range from 40 to 90% is enough for osteointegration (Karageorgiou and Kaplan, 2005). Hence, it is noteworthy that the computed porosities show potential for biomedical applications.

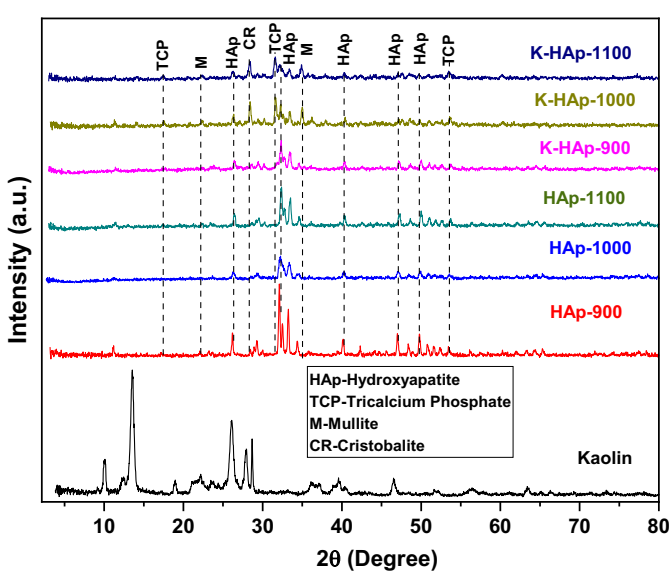

Fig. 8. X-ray diffraction patterns of Kankara kaolin, non-reinforced HAp and K-HAp powders.

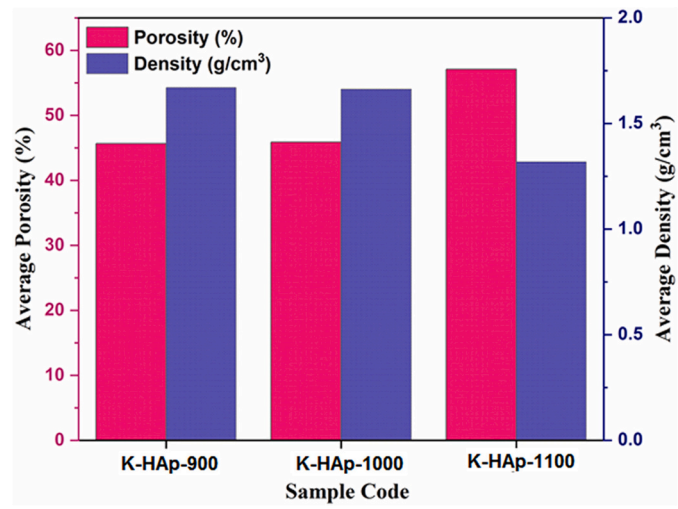

Fig. 9. Variation of the average porosity and density of K-HAp scaffolds.

Porosities of HAp samples (HAp 900–1100) and RB (raw bone) have been reported in a previous study (Obada et al., 2020a). The porosities of these samples varied from 46.9 ± 0.10% to 60.2 ± 0.76% with porosity value of HAp-1100 (60.2%) slightly higher than K-HAp-1100 (59.2%). This could be ascribed to the kaolin particles used as reinforcement which may have marginally filled some of the pores.

Apparent density for the kaolin reinforced samples was found in the range between 1.32 ± 0.01 and 1.67 ± 0.01 g/cm^3. The K-HAp 1100 sample was denser as compared to other samples as a result of the highest sintering temperature used for its densification. This may have been possible due to the encapsulation of smaller pores in larger ones with consequent increase in densely packed regions in the bulk. It is still not very clear why this is the case as the K-HAp-1100 sample had the highest porosity, however smaller pores in the bulk being absorbed into larger pores could be noteworthy.

3.8. Compressive strengths of the K-HAp pellets

It is important to highlight the robust compressive strength of the pellets after reinforcing with micro-sized kaolin particles and applying the low cold compaction pressure (1 MPa) as compared to non-reinforced HAp pellets. Significant compressive strength of 7.66 MPa as compared with 0.89 MPa for the non-reinforced HAp matrix was observed at 1100 °C. Fig. 10 reveals that the compressive strength measured exhibited gradients for all the samples. By using a low cold compaction pressure of 1 MPa, the range of compressive strength for all the samples were 5.67 ± 0.15 MPa, to 7.66 ± 0.14 MPa. The compressive strength of the K-HAp-1100 was significantly increased with compaction pressure of 1 MPa and surpassed the minimum mechanical strength requirements of trabecular bone (about 2 MPa) making it suitable for bone regeneration. Emphasizing the need for the compaction pressure, the pellets fabricated without compaction pressure gave compressive strengths of 1.98 ± 0.08 MPa; 1.97 ± 0.16 MPa and 0.89 ± 0.08 MPa, for K-HAp-900, 1000 and 1100 samples, respectively. These values did not reach the minimum mechanical strength requirements of trabecular bone (about 2 MPa).

The analysis of variance (ANOVA) of the three groups of compacted K-HAp variants [K-HAp 900(C), K-HAp 1000(C), and K-HAp 1100(C); please see Fig. 11] as depicted in Table 2 show that the obtained F_o value of 9.333 is greater than the cut-off value of 5.143 from the F distribution with 2 and 6 degrees of freedom and a significance level of 0.05. Therefore, the null hypothesis that states that the mean levels, as obtained from the compressive test experiments conducted in triplicates, are the same is rejected. From this analysis, it can be stated that the sintering temperature has an effect on the compressive strength of the

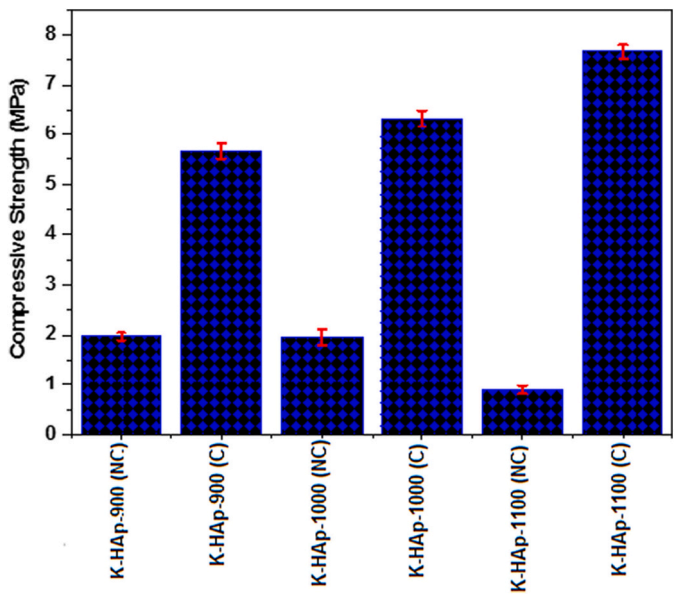

Fig. 10. Compressive strength of HAp and K-HAp scaffolds; NC- no compaction pressure; C- I MPa compaction pressure.

compacted samples.

In a similar vein, the analysis of variance of the three groups as shown in Table 3, which is representattive of the non-compacted K-HAp variants [K-HAp 900(NC), K-HAp 1000(NC), and K-HAp 1100(NC); please see Fig. 11], show that the obtained F_o value of 101.826 is greater than the cut-off value of 5.143 from the F distribution with 2 and 6 degrees of freedom and a significance level of 0.05. Therefore, the null hypothesis that states that the mean levels, as obtained from the compressive test experiments conducted in triplicates, are the same is rejected. From this analysis, it can be stated that the sintering temperature has an effect on the compressive strength of the non-compacted samples.

One reason for the improved compressive strength with the influence of temperature can be ascribed to the "particle-reinforcing" effect of kaolin. The well dispersed kaolin formed good bridging with the HAp. Based on the studies reported on the compressive strength of human trabecular bone (Jones et al., 2006; White et al., 2007; Fu et al., 2013), the kaolin reinforced bioceramic material can be used as bone implants in a fractured area of trabecular bone. The compaction pressure used for pelletizing the K-HAp scaffolds enhanced the densification of the scaffolds. The compressive strengths of the compacts increased with temperature because with an increase in temperature, the ultimate stress of the ceramic compacts decrease, while the strain corresponding to the peak strength increase. The well-defined crystal structures of the kaolin reinforced hydroxyapatite indicated the quality of the bioceramic materials for trabecular bone applications, and this was also reported by Rollo et al. (2015).

3.9. Biodegradability (weight loss) and pH variation profiles of the kaolin reinforced samples

Fig. 12 represents the weight loss profiles of the scaffolds over time in phosphate buffer saline (PBS). For all the pelletized bioceramic materials, there was an initial increase in weight in the first three days before the weight steadily decreased with incubation time. The K-HAp-1100 bioceramic material exhibited a slower degradation rate than the other scaffolds, which may be associated with the inherent porosity that slowed down the degradation of weight of the bioceramic materials.

The pH profiles for the PBS-soaked scaffolds as illustrated in Fig. 13 show that the pH value of the PBS solution gradually increased for all the bioceramic materials at an earlier stage, while for the K-HAP-1100 sample, there was a steady increase in pH during the 21 days of incubation. There was a considerable increase of pH for the K-HAp-900 scaffold which hovered around the neutral pH levels. Such gradients in pH rise may be ascribed to the dissolution of alkaline ions from the kaolin reinforced pellets, and this compensates the acidity of the PBS medium, locally. The pH auto-regulation mechanism shown by the K-HAp-900 scaffold due to presumably more alkaline ions in the bulk of the samples can be quite efficient in reducing the inflammation of soft and hard tissues surrounding the scaffold during in vivo implantation.

Table 2
One-Way ANOVA on the impact of sintering temperature on the compressive strength of compacted K-HAp scaffolds.

	Sum of squares	df	Mean square	F	Sig.
Between Groups	6.222	2	3.111	9.333	0.014
Within Groups	2.000	6	0.333		
Total	8.222	8			

Table 3
One-way ANOVA on the impact of sintering temperature on the compressive strength of non-compacted K-HAp scaffolds.

	Sum of squares	df	Mean square	*F*	Sig.
Between Groups	2.464	2	1.232	101.826	0.000
Within Groups	0.073	6	0.012		
Total	2.537	8			

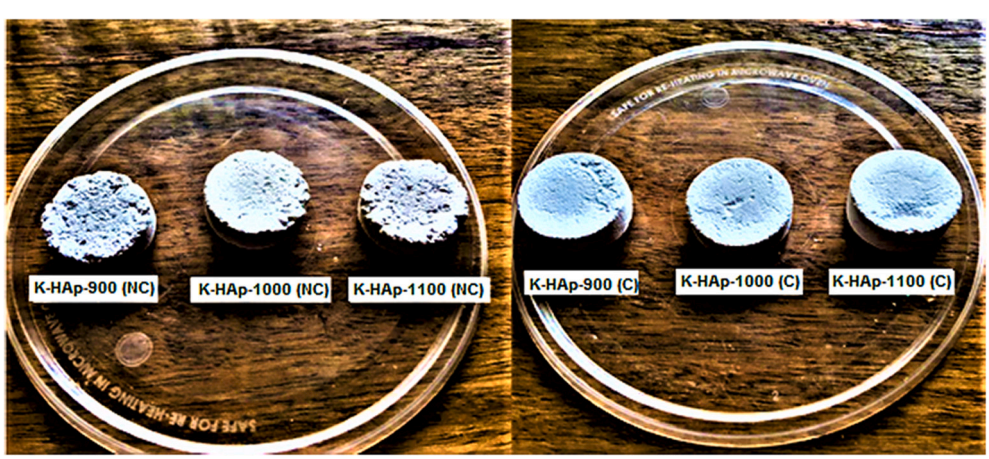

Fig. 11. Pictures of the non-compacted (NC) and compacted (C) samples.

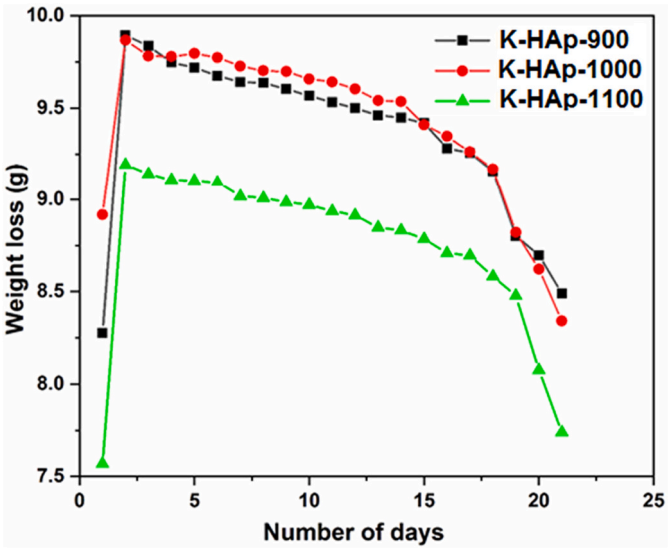

Fig. 12. Weight loss profiles of the kaolin reinforced samples (K-HAp-900, 1000, and 1100).

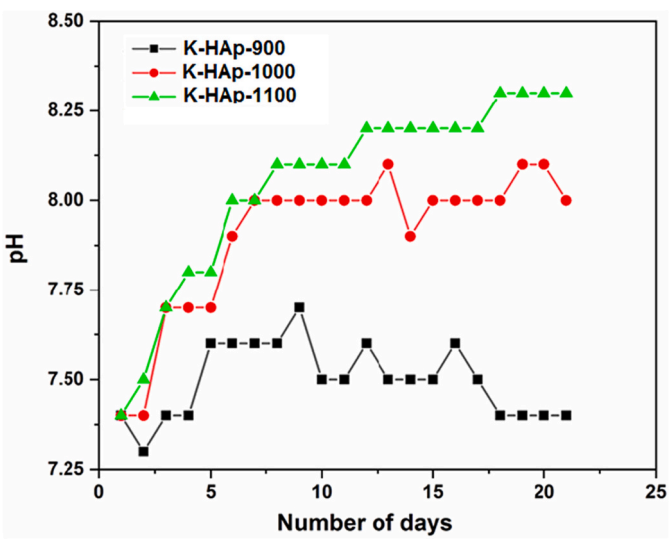

Fig. 13. pH variation profiles of the kaolin reinforced samples (K-HAp-900, 1000, and 1100).

3.10. Antibacterial activity of the reinforced scaffolds

Typically, bacterial and fungal colonies can quickly grow on HAp due to their bioactive properties and the presence of calcium and phosphate ions which supplement as nutrients for their growth. The formation of these colonies is a major reason for implant failure, and, therefore, it is an important parameter to study. The K-HAp-900 sample (Fig. 14) showed bactericidal effect on gram negative E.coli with inhibition diameters reaching a maximum at 11 ± 0.5 mm. However, no such activity was observed for all the other bacterial and viral strains. The activity exhibited for bacterial strain (E.coli) by the K-HAp-900 scaffold can be ascribed to the variations in the cell structure, the rate of diffusion, the metabolism, and the interaction of the microparticles with the microorganisms. This antibacterial effect can also be linked to the pH auto-regulation potentials of K-HAp-900, as the rate of metabolism is a bit stable. It is possible that the antibacterial activity of the sample and other kaolin reinforced variants can be further improved by doping with trace metal ions as shown in studies reported by Tank et al. (2011, 2014), and Obada et al. (2021b) with a protocol which will be safe to use for biomedical applications.

3.11. Morphology of scaffolds after immersion in SBF and representative Ca/P ratios

The pH auto-regulation potential and the antimicrobial activity of K-HAp-900 bioceramic material necessitated a further study on its in-vitro compatibility potential. The morphology of the scaffolds after immersion in SBF for 0, 14, and 28 days is displayed in Fig. 15. Some parts of the surface of the kaolin reinforced hydroxyapatite were covered with an apatite layer after 14 days as there is a distinct topography and morphology as compared to bioceramic materials not immersed in SBF. On the 28th day, the surface of the hydroxyapatite is also distinct and the agglomeration is higher as compared to the microstructure on the 14th day. The apatite formation on the scaffold started to grow individually and separately from each other on the 14th day. On the 28th day, a process of cluster agglomeration started with the consequent losing of individual clusters. These trends were also noticed in a related work conducted by Abad-Javier et al. (2018).

The variation of Ca/P ratio after the in vitro evaluation tests in SBF is presented in Fig. 16. For all scaffolds, Ca/P ratio in weight and atomic percentages decreased with incubation time, higher in weight percent than the stoichiometric value of apatite (Ca/P = 1.67). This indicates that the surface was covered by a Ca rich-apatite layer as depicted by the microstructures. After 14 and 28 days, the atomic Ca/P ratio for both K-HAp-1000 &1100 exhibited ratios equal to 1.48 and 1.39, respectively, which shows calcium-deficiency in the hydroxyapatite bulk. This result indicated that the SBF favours the degradation process after 14 days for

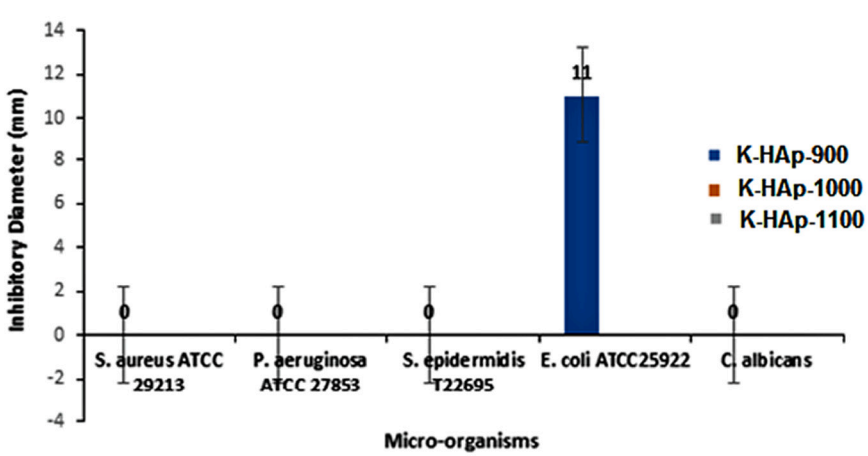

Fig. 14. Inhibitory diameters of the K-HAp powders on the tested microbial strains.

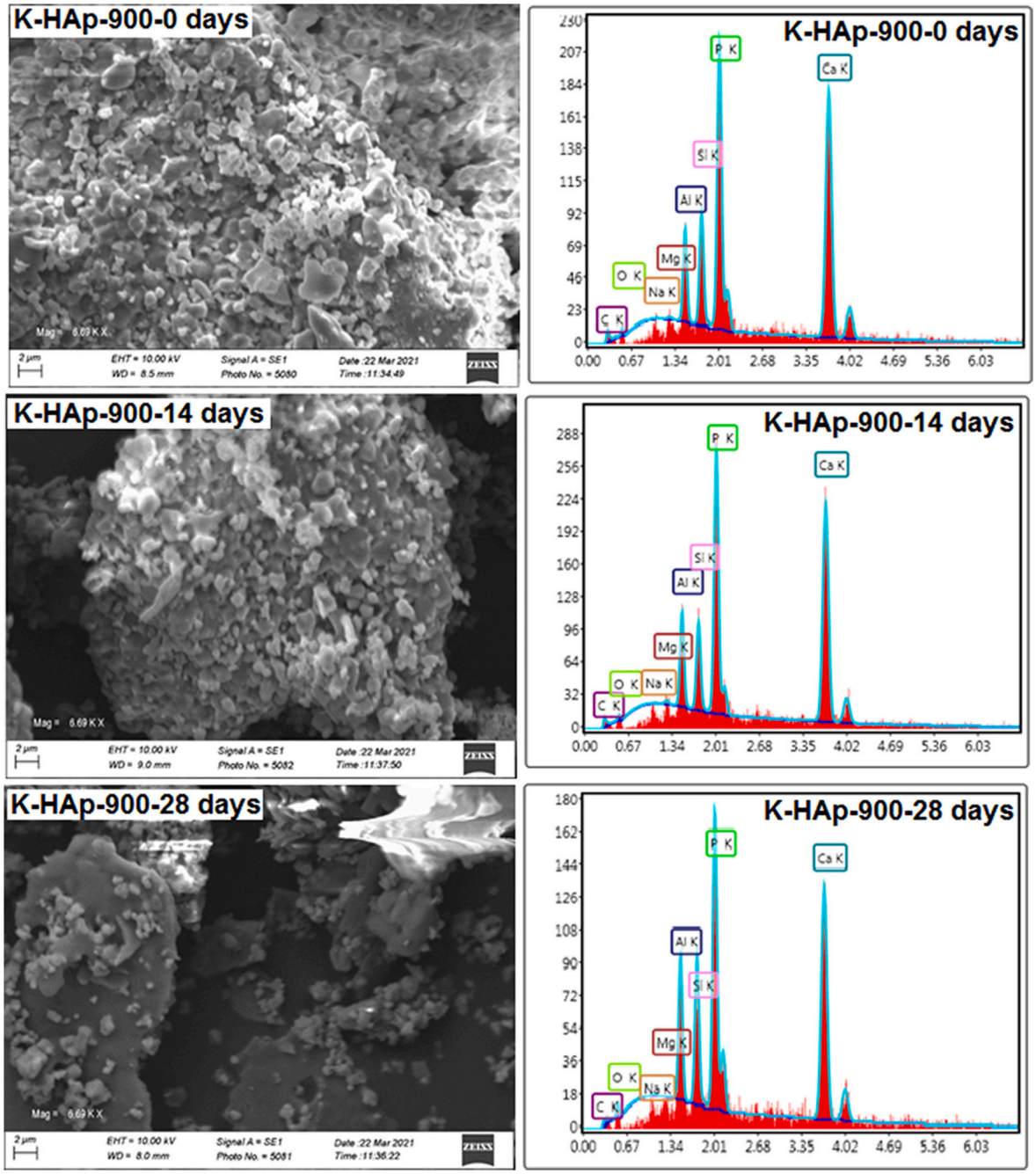

Fig. 15. Morphology of the K-HAp-900 scaffolds after immersion in simulated body fluid (SBF).

the scaffolds with osteoinductive support potentials for bone regeneration.

4. Discussion

To fabricate bioceramic scaffolding materials with a hierarchical structure, the sol-gel technique followed by heat treatment was used to produce the kaolin reinforced bioceramic material with a combined micro, macro and mesoporous structure. The trimodal porous structure as illustrated in the SEM images (Fig. 7), which were interconnected in nature, could be instrumental for the enhancement of nutrient exchange, cell proliferation, promotion of bone formation and bone/tissue ingrowth. This assertion is in line with several researchers who have produced bioceramic materials with various structures for biomedical applications (Zhao et al., 2015; Vallet-Regí et al., 2016; Gu et al., 2017). The SEM images of the kaolin reinforced scaffolds show that a bioceramic scaffold with a trimodal architecture was fabricated, which is close to the structural characteristics of natural bone. This is therefore a versatile scaffolding material to support bone regeneration.

The synthesized kaolin reinforced composite scaffolds show mechanical robustness, and tailorable degradation rates. A quick degradation of scaffolding materials usually doesn't allow enough time for the bone to grow quickly enough and ensure completeness in bone repair applications. Essentially, it is quite important for an orthopaedic biodegradable implant to have a degradation rate that matches the healing or regeneration process of blood vessels (Xie et al., 2016; Zhu et al., 2019).On the other hand, if the degradation is too slow, it may not provide enough space for new bone ingrowth. Therefore, it can be suggested that the fabricated bioceramic scaffolding materials have characteristics in an acceptable range. The K-HAp scaffolds showed

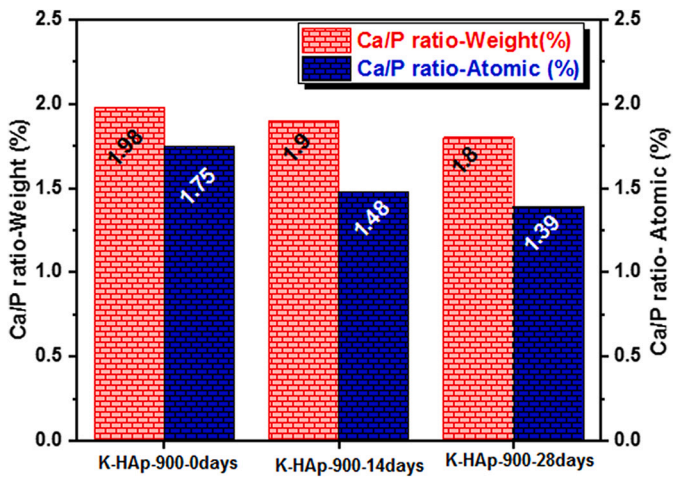

Fig. 16. Ca/P ratio of K-HAp-900 samples after immersion in simulated body fluid (SBF) for 28 days.

moderate degradation and auto-pH regulation tendencies. The compressive strength of the low-cold compacted scaffolds showed matchable properties with the mechanical requirements of the trabecular bone (2–12 MPa). To compare the mechanical properties of the scaffolds in this study to other studies can be misleading. This is because many factors influence the mechanical properties of hydroxyapatite derived scaffolds. These factors are pore size, and orientation, material purity, sintering temperature and time, phase transitions and phases present, and the volume of sample. To put into context, Metsger et al. (1999) conducted a detailed comparison of studies on mechanical properties of HAp and reported, for example, that the compressive strength of dense HAp ranged from 100 to 900 MPa. Other parameters which may have endowed the dense HAp with this robust compressive strength may not have been mentioned and this may not allow an accurate comparison. Hence, the compressive strength of the pellets/scaffolds with trimodal architecture synthesized in this study have not been compared to properties of HAp derived scaffolds reported in the literature. However, the properties of the produced scaffolds have been compared to the properties of bone since the intended application for the bioceramic materials studied here is as bone substitutes. The considerations when conducting the characteristics of these scaffolds to bone include: the materials degrade slowly and when a comparison of this nature is made, it is important to consider that the strength and stiffness would increase with bone ingrowth. Secondly, the flexibility of the method of fabrication allows the characteristics of the scaffolds to be tuned to enhance the compactness and strength of the scaffolds. Normally, the strength of a degradable scaffold should match that of the host bone. Essentially, for scaffolding materials that degrade slowly, for instance, HAp, it is important that the characteristics of the scaffold and the ingrown bones match that of the native bone. The scaffolding materials prepared in this study had average compressive strength of 5.67 to 7.66 MPa, which is close to the 1–7 MPa range of strengths reported for trabecular bone by Bayraktar et al. (2004),

The immersion assays conducted in-vitro in simulated body fluid suggested that the reinforced samples accelerated the growth and nucleation of new phases. This effect can be ascribed to the dissolution of the scaffolds which triggered the release of Ca^{2+} which is essential for CaP nucleation and favours the formations of new HAp phase as shown in the Ca/P ratios after immersion.

The limitations in this study include the inability to test, in vitro, the non-reinforced scaffolds alongside the reinforced variants. Also, a standalone kaolin scaffold would have been used as a positive control. An in-depth study will be performed in vitro and in vivo specifically for antibacterial, acute, and chronic toxicity evaluations to further demonstrate the potential for clinical applications.

5. Conclusions

This study has shown the feasibility and viability of producing hydroxyapatite from animal bones and further reinforcing with kaolin to fabricate scaffolds through a low-cold compaction protocol assisted by heat treatment. The crystallites of kaolin and kaolin reinforced microparticles were mainly comprised of 40–65 nm sized particles which has similarities with natural bone apatite. The calcium to phosphate ratio of K-HAp was 1.66 which is very close to 1.67 (the Ca/P ratio for stoichiometric hydroxyapatite). The micropore volumes of the samples, 0.000397, 0.001287 and 0.000334 cm^3/g, for KHAp 900–1100, respectively, are in line with data obtained for bioactive materials in other studies. The grain morphology as revealed by TEM analyses showed that the spherical orientation of the samples has the potential of enhancing the mechanical properties of the kaolin-reinforced scaffolds. From the X-ray diffraction analyses of the sintered scaffolding materials in comparison with pure HAp and kaolin, the reflections of tri-calcium phosphate (β-TCP) which was evident in the kaolin reinforced mix sintered at 1100 °C (K-HAp-1100), has the tendency to enhance accelerated new bone formation if the scaffolds are used as implants. In addition, K-HAp-1100 prepared with 1 MPa compaction pressure showed the most significant compressive strength of 7.66 MPa. In-vitro experiments showed the degradability and compatibility of the scaffolds as a relative neutral pH was maintained for the K-HAp-900 sample. Moreover, sample K-HAp-900 also showed inhibitory potentials for *E. coli*. In the current study, the K-HAp-900 scaffold prepared through an innovative strategy possess a better combination of physical, biological and mechanical characteristics (5.66 MPa compressive strength). Essentially, the novel compaction protocol and kaolin reinforcement used in this study represents a new approach to fabricate biomimicking scaffolds for bone regeneration.

Declaration of Competing Interest

None.

Acknowledgement

The authors wish to acknowledge TETFund Nigeria for supporting this research under grant Ref: NRF_SETI_HSW_00714, 2020.

References

Abad-Javier, M.E., Nuñez-Anita, R.E., Cajero-Juárez, M., Contreras-García, M.E., 2018. Comparability in bioactivity assays of 45s5 bioglass scaffolds using simulated body fluid and rabbit blood plasma. J. Pharm. Biol. Sci. 13, 13–23.

Abifarin, J.K., Obada, D.O., Dauda, E.T., Dodoo-Arhin, D., 2019. Experimental data on the characterization of hydroxyapatite synthesized from biowastes. Data Brief 26, 104485.

Akpan, E.S., Dauda, M., Kuburi, L.S., Obada, D.O., Dodoo-Arhin, D., 2020a. A comparative study of the mechanical integrity of natural hydroxyapatite scaffolds prepared from two biogenic sources using a low compaction pressure method. Res. Phys. 17, 103051.

Akpan, E.S., Dauda, M., Kuburi, L.S., Obada, D.O., 2020b. A facile synthesis method and fracture toughness evaluation of catfish bones-derived hydroxyapatite. MRS Adv. 5 (26), 1357–1366.

Akpan, E.S., Dauda, M., Kuburi, L.S., Obada, D.O., 2021a. Box-Behnken experimental design for the process optimization of catfish bones derived hydroxyapatite: a pedagogical approach. Mater. Chem. Phys. 272, 124916.

Akpan, E.S., Dauda, M., Kuburi, L.S., Obada, D.O., Bansod, N.D., Dodoo-Arhin, D., 2021b. Hydroxyapatite ceramics prepared from two natural sources by direct thermal conversion: from material processing to mechanical measurements. Mat. Today: Proc. 38, 2291–2294.

Ayed, F.B., Bouaziz, J., Bouzouita, K., 2001. Calcination and sintering of fluorapatite under argon atmosphere. J. Alloys Compd. 322 (1–2), 238–245.

Ballet, T., Boulange, L., Brechet, Y., Bruckert, F., Weidenhaupt, M., 2010. Protein conformational changes induced by adsorption onto material surfaces: an important issue for biomedical applications of material science. Bul. Pol. Acad. Sci. Tech. Sci. 58 (2), 303–315.

Bauer, A.T., 1966. Antibiotic susceptibility testing by a standardized single disc method. Am. J. Clin. Pathol. 45, 149–158.

Bayraktar, H.H., Morgan, E.F., Niebur, G.L., Morris, G.E., Wong, E.K., Keaveny, T.M., 2004. Comparison of the elastic and yield properties of human femoral trabecular and cortical bone tissue. J. Biomech. 37 (1), 27–35.

Belhouchet, H., Chouia, F., Hamidouche, M., Leriche, A., 2016. Preparation and characterization of anorthite and hydroxyapatite from Algerian kaolin and natural phosphate. J. Therm. Anal. Calorim. 126 (3), 1045–1057.

Bergaya, F., Lagaly, G., 2013. Handbook of Clay Science. Newnes.

Bohor, B.F., Hughes, R.E., 1971. Scanning electron microscopy of clays and clay minerals. Clay Clay Miner. 19, 49–54.

Chavan, P.N., Bahir, M.M., Mene, R.U., Mahabole, M.P., Khairnar, R.S., 2010. Study of nanobiomaterial hydroxyapatite in simulated body fluid: formation and growth of apatite. Mater. Sci. Eng. B 168 (1–3), 224–230.

Dean, J.C., Tisdel, C.L., Goldberg, V.M., Parr, J., Davy, D., Stevenson, S., 1995. Effects of hydroxyapatite tricalcium phosphate coating and intracancellous placement on bone ingrowth in titanium fibermetal implants. J. Arthroplast. 10 (6), 830–838.

Farzadi, A., Solati-Hashjin, M., Bakhshi, F., Aminian, A., 2011. Synthesis and characterization of hydroxyapatite/β-tricalcium phosphate nanocomposites using microwave irradiation. Ceram. Int. 37 (1), 65–71.

Farzadi, A., Bakhshi, F., Solati-Hashjin, M., Asadi-Eydivand, M., abu Osman, N. A., 2014. Magnesium incorporated hydroxyapatite: synthesis and structural properties characterization. Ceram. Int. 40 (4), 6021–6029.

Fu, Q., Saiz, E., Rahaman, M.N., Tomsia, A.P., 2013. Toward strong and tough glass and ceramic scaffolds for bone repair. Adv. Funct. Mater. 23 (44), 5461–5476.

Goyanes, A., Souto, C., Martínez-Pacheco, R., 2013. Chitosan–kaolin coprecipitate as disintegrant in microcrystalline cellulose-based pellets elaborated by extrusion–spheronization. Pharm. Dev. Technol. 18 (1), 137–145.

Gu, Z., Wang, S., Weng, W., Chen, X., Cao, L., Wei, J., Su, J., 2017. Influences of doping mesoporous magnesium silicate on water absorption, drug release, degradability, apatite-mineralization and primary cells responses to calcium sulfate based bone cements. Mater. Sci. Eng. C 75, 620–662.

Haberko, K., Bućko, M.M., Brzezińska-Miecznik, J., Haberko, M., Mozgawa, W., Panz, T., Zarębski, J., 2006. Natural hydroxyapatite—its behaviour during heat treatment. J. Eur. Ceram. Soc. 26 (4–5), 537–542.

Harabi, A., Harabi, E., Chehlatt, S., Zouai, S., Karboua, N.E., Foughali, L., 2016. Effect of B_2O_3 on mechanical properties of porous natural hydroxyapatite derived from cortical bovine bones sintered at 1,050 C. Desalin. Water Treat. 57 (12), 5303–5309.

Heidari, F., Razavi, M., Bahrololoom, M.E., Bazargan-Lari, R., Vashaee, D., Kotturi, H., Tayebi, L., 2016. Mechanical properties of natural chitosan/hydroxyapatite/magnetite nanocomposites for tissue engineering applications. Mater. Sci. Eng. C 65, 338–344.

Hongquan, Z., Yuhua, Y., Youfa, W., Shipu, L., 2003. Morphology and formation mechanism of hydroxyapatite whiskers from moderately acid solution. Mater. Res. 6 (1), 111–115.

Jones, J.R., Ehrenfried, L.M., Hench, L.L., 2006. Optimising bioactive glass scaffolds for bone tissue engineering. Biomaterials 27 (7), 964–973.

Kakali, G., Perraki, T.H., Tsivilis, S., Badogiannis, E., 2001. Thermal treatment of kaolin: the effect of mineralogy on the pozzolanic activity. Appl. Clay Sci. 20 (1–2), 73–80.

Karageorgiou, V., Kaplan, D., 2005. Porosity of 3D biomaterial scaffolds and osteogenesis. Biomaterials 26 (27), 5474–5491.

Kikuchi, M., Itoh, S., Ichinose, S., Shinomiya, K., Tanaka, J., 2001. Self-organization mechanism in a bone-like hydroxyapatite/collagen nanocomposite synthesized in vitro and its biological reaction in vivo. Biomaterials 22 (13), 1705–1711.

Kokubo, T., Takadama, H., 2006. How useful is SBF in predicting in vivo bone bioactivity? Biomaterials 27 (15), 2907–2915.

Kusakabe, A., Hirota, K., Mizutani, T., 2017. Crystallisation of hydroxyapatite in phosphorylated poly(vinyl alcohol) as a synthetic route to tough mechanical hybrid materials. Mater. Sci. Eng. C 70, 487–493. https://doi.org/10.1016/j.msec.2016.09.006.

Landi, E., Tampieri, A., Celotti, G., Sprio, S., 2000. Densification behaviour and mechanisms of synthetic hydroxyapatites. J. Eur. Ceram. Soc. 20 (14–15), 2377–2387.

Laonapakul, T., Sutthi, R., Chaikool, P., Talangkun, S., Boonma, A., Chindaprasirt, P., 2021. Calcium phosphate powders synthesized from CaCO3 and CaO of natural origin using mechanical activation in different media combined with solid-state interaction. Mater. Sci. Eng. C 118, 111333.

Law, M.F.L., Deasy, P.B., 1997. Effect of common classes of excipients on extrusion-spheronization. J. Microencapsul. 14 (5), 647–657.

Lee, S., Kim, Y.J., Moon, H.S., 2003. Energy-filtering transmission electron microscopy (EFTEM) study of a modulated structure in metakaolinite, represented by a 14 °A modulation. J. Am. Ceram. Soc. 86, 174–176.

Li, H., Gong, M., Yang, A., Ma, J., Li, X., Yan, Y., 2012. Degradable biocomposite of nano calcium-deficient hydroxyapatite-multi (amino acid) copolymer. Int. J. Nanomedicine 7, 1287.

Lin, K., Chang, J., Cheng, R., Ruan, M., 2007. Hydrothermal microemulsion synthesis of stoichiometric single crystal hydroxyapatite nanorods with mono-dispersion and narrow-size distribution. Mater. Lett. 61 (8–9), 1683–1687.

Lowe, B., Venkatesan, J., Anil, S., Shim, M.S., Kim, S.K., 2016. Preparation and characterization of chitosan-natural nano hydroxyapatite-fucoidan nanocomposites for bone tissue engineering. Int. J. Biol. Macromol. 93, 1479–1487.

Mallick, S., Pattnaik, S., Swain, K., De, P.K., Saha, A., Ghoshal, G., Mondal, A., 2008. Formation of physically stable amorphous phase of ibuprofen by solid state milling with kaolin. Eur. J. Pharm. Biopharm. 68 (2), 346–351.

Metsger, D.S., Rieger, M.R., Foreman, D.W., 1999. Mechanical properties of sintered hydroxyapatite and tricalcium phosphate ceramic. J. Mater. Sci. Mater. Med. 10 (1), 9–17.

Munar, M.L., Udoh, K.I., Ishikawa, K., Matsuya, S., Nakagawa, M., 2006. Effects of sintering temperature over 1,300 C on the physical and compositional properties of porous hydroxyapatite foam. Dent. Mater. J. 25 (1), 51–58.

Murugan, R., Ramakrishna, S., Rao, K.P., 2006. Nanoporous hydroxy-carbonate apatite scaffold made of natural bone. Mater. Lett. 60 (23), 2844–2847.

Obada, D.O., Dodoo-Arhin, D., Dauda, M., Anafi, F.O., Ahmed, A.S., Ajayi, O.A., 2016a. Potentials of fabricating porous ceramic bodies from kaolin for catalytic substrate applications. Appl. Clay Sci. 132, 194–204.

Obada, D.O., Dodoo-Arhin, D., Dauda, M., Anafi, F.O., Ahmed, A.S., Ajayi, O.A., Samotu, I.A., 2016b. Effect of mechanical activation on mullite formation in an alumina-silica ceramics system at lower temperature. World J. Eng. 13 (4), 288–293.

Obada, D.O., Dodoo-Arhin, D., Dauda, M., Anafi, F.O., Ahmed, A.S., Ajayi, O.A., Samotu, I.A., 2016c. Physical and mechanical properties of porous kaolin based ceramics at different sintering temperatures. West Indian J. Eng. 39 (1).

Obada, D.O., Dodoo-Arhin, D., Dauda, M., Anafi, F.O., Ahmed, A.S., Ajayi, O.A., 2017a. Physico-mechanical and gas permeability characteristics of kaolin based ceramic membranes prepared with a new pore-forming agent. Appl. Clay Sci. 150, 175–183.

Obada, D.O., Dodoo-Arhin, D., Dauda, M., Anafi, F.O., Ahmed, A.S., Ajayi, O.A., 2017b. The impact of kaolin dehydroxylation on the porosity and mechanical integrity of kaolin based ceramics using different pore formers. Res. Phys. 7, 2718–2727.

Obada, D.O., Dodoo-Arhin, D., Dauda, M., Anafi, F.O., Ahmed, A.S., Ajayi, O.A., 2017c. Pressureless sintering and gas flux properties of porous ceramic membranes for gas applications. Res. Phys. 7, 3838–3846.

Obada, D.O., Dauda, E.T., Abifarin, J.K., Dodoo-Arhin, D., Bansod, N.D., 2020a. Mechanical properties of natural hydroxyapatite using low cold compaction pressure: effect of sintering temperature. Mater. Chem. Phys. 239, 122099.

Obada, D.O., Dodoo-Arhin, D., Dauda, M., Anafi, F.O., Ahmed, A.S., Ajayi, O.A., Momoh, O.J., 2020b. Crack behaviour and mechanical properties of thermally treated kaolin-based ceramics: the influence of pore generating agents. Appl. Clay Sci. 194, 105698.

Obada, D.O., Dauda, E.T., Abifarin, J.K., Bansod, N.D., Dodoo-Arhin, D., 2021a. Mechanical measurements of pure and kaolin reinforced hydroxyapatite-derived scaffolds: a comparative study. Mat. Today: Proc. 38, 2295–2300.

Obada, D.O., Salami, K.A., Oyedeji, A.N., Fasanya, O.O., Suleiman, M.U., Ibisola, B.A., Dauda, E.T., 2021b. Solution combustion synthesis of strontium-doped hydroxyapatite: effect of sintering and low compaction pressure on the mechanical properties and physiological stability. Mater. Lett. 130613.

Okafor, E., Obada, D.O., Dodoo-Arhin, D., 2020. Ensemble learning prediction of transmittance at different wavenumbers in natural hydroxyapatite. Sci. African 9, e00516.

Okafor, E., Obada, D.O., Ibrahim, Y., Dodoo-Arhin, D., 2021. Prediction of the reflection intensity of natural hydroxyapatite using generalized linear model and ensemble learning methods. Eng. Rep. 3 (2), e12292.

Pang, Y.X., Bao, X., 2003. Influence of temperature, ripening time and calcination on the morphology and crystallinity of hydroxyapatite nanoparticles. J. Eur. Ceram. Soc. 23 (10), 1697–1704.

Pramanik, S., Agarwal, A.K., Rai, K.N., 2005. Development of high strength hydroxyapatite for hard tissue replacement. Trends Biomater. Artif. Organs 19 (1), 46–51.

Pramanik, S., Agarwal, A.K., Rai, K.N., Garg, A., 2007. Development of high strength hydroxyapatite by solid-state-sintering process. Ceram. Int. 33 (3), 419–426.

Ramesh, S., Loo, Z.Z., Tan, C.Y., Chew, W.K., Ching, Y.C., Tarlochan, F., Sarhan, A.A., 2018. Characterization of biogenic hydroxyapatite derived from animal bones for biomedical applications. Ceram. Int. 44 (9), 10525–10530.

Rollo, J.M.D.A., Boffa, R.S., Cesar, R., Schwab, D.C., Leivas, T.P., 2015. Assessment of trabecular bones microarchitectures and crystal structure of hydroxyapatite in bone osteoporosis with application of the Rietveld method. Proc. Eng. 110, 8–14.

Rusu, V.M., Ng, C.H., Wilke, M., Tiersch, B., Fratzl, P., Peter, M.G., 2005. Size-controlled hydroxyapatite nanoparticles as self-organized organic–inorganic composite materials. Biomaterials 26 (26), 5414–5426.

Scherrer, P., 1918. Estimation of the size and internal structure of colloidal particles by means of Röntgen. Nachr. Ges. Wiss. Göttingen 2, 96–100.

Sopyan, I., Kaur, J., 2009. Preparation and characterization of porous hydroxyapatite through polymeric sponge method. Ceram. Int. 35 (8), 3161–3168.

Suchanek, W., Yashima, M., Kakihana, M., Yoshimura, M., 1996. Processing and mechanical properties of hydroxyapatite reinforced with hydroxyapatite whiskers. Biomaterials 17 (17), 1715–1723.

Sun, Y., Guo, G., Wang, Z., Guo, H., 2006. Synthesis of single-crystal HAP nanorods. Ceram. Int. 32 (8), 951–954.

Sutthi, R., Kaewwinud, N., Chindaprasirt, P., Mutoh, Y., Laonapakul, T., 2018. Effect of curing temperature and time on the mechanical properties of hydroxyapatite/calcined kaolin. ScienceAsia 44, 397–402.

Tang, W., Yuan, Y., Lin, D., Niu, H., Liu, C., 2014. Kaolin-reinforced 3D MBG scaffolds with hierarchical architecture and robust mechanical strength for bone tissue engineering. J. Mater. Chem. B 2 (24), 3782–3790.

Tank, K.P., Sharma, P., Kanchan, D.K., Joshi, M.J., 2011. FTIR, powder XRD, TEM and dielectric studies of pure and zinc doped nano-hydroxyapatite. Cryst. Res. Technol. 46 (12), 1309–1316.

Tank, K.P., Chudasama, K.S., Thaker, V.S., Joshi, M.J., 2014. Pure and zinc doped nano-hydroxyapatite: synthesis, characterization, antimicrobial and hemolytic studies. J. Cryst. Growth 401, 474–479.

Usmaniya, U.M., Thampi, V.A., Subramanian, B., 2019. Electrophoretic deposition of bioactive glass-nanoclay nanocomposites on titanium. Appl. Clay Sci. 167, 1–8.

Vaiana, C.A., Leonard, M.K., Drummy, L.F., Singh, K.M., Bubulya, A., Vaia, R.A., Kadakia, M.P., 2011. Epidermal growth factor: layered silicate nanocomposites for tissue regeneration. Biomacromolecules 12 (9), 3139–3146.

Vallet-Regí, M., Salinas, A.J., Arcos, D., 2016. Tailoring the structure of bioactive glasses: from the nanoscale to macroporous scaffolds. Int. J. Appl. Glas. Sci. 7 (2), 195–205.
Véliz, D.S., Alam, C., Toivola, D.M., Toivakka, M., Alam, P., 2014. On the non-linear attachment characteristics of blood to bacterial cellulose/kaolin biomaterials. Colloids Surf. B: Biointerfaces 116, 176–182.
White, A.A., Best, S.M., Kinloch, I.A., 2007. Hydroxyapatite–carbon nanotube composites for biomedical applications: a review. Int. J. Appl. Ceram. Technol. 4 (1), 1–13.
Xie, G., Takada, H., Kanetaka, H., 2016. Development of high performance MgFe alloy as potential biodegradable materials. Mater. Sci. Eng. A 671, 48–53.
Zhao, S., Zhang, J., Zhu, M., Zhang, Y., Liu, Z., Ma, Y., Zhang, C., 2015. Effects of functional groups on the structure, physicochemical and biological properties of mesoporous bioactive glass scaffolds. J. Mater. Chem. B 3 (8), 1612–1623.
Zhao, X., Zhang, L., Wang, X., Yang, J., He, F., Wang, Y., 2018. Preparation and mechanical properties of controllable orthogonal arrangement of carbon fiber reinforced hydroxyapatite composites. Ceram. Int. 44 (7), 8322–8333.
Zhao, X.Y., Zhu, Y.J., Chen, F., Lu, B.Q., Wu, J., 2013. Nanosheet-assembled hierarchical nanostructures of hydroxyapatite: surfactant-free microwave-hydrothermal rapid synthesis, protein/DNA adsorption and pH-controlled release. CrystEngComm 15 (1), 206–212.
Zhu, W., Chu, C., Kuddannaya, S., Yuan, Y., Walczak, P., Singh, A., Bulte, J.W., 2019. In vivo imaging of composite hydrogel scaffold degradation using CEST MRI and two-color NIR imaging. Adv. Funct. Mater. 29 (36), 1903753.